Journal of
Materials Chemistry C

Materials for optical, magnetic and electronic devices

Accepted Manuscript

This article can be cited before page numbers have been issued, to do this please use: S. Li, L. Zhou, X. Shen, Y. Gu, Y. Tang and M. Wang, *J. Mater. Chem. C*, 2025, DOI: 10.1039/D5TC02429C.

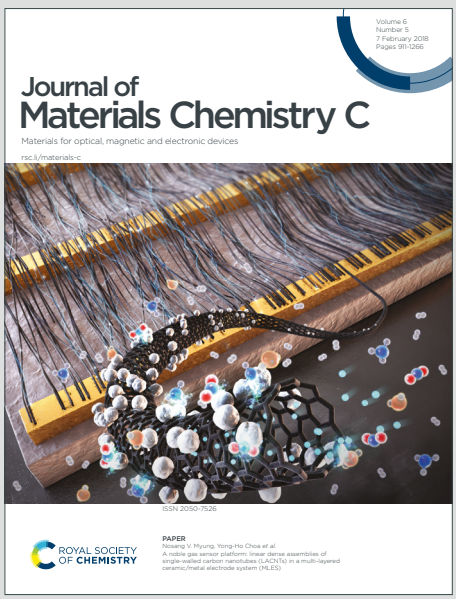

ROYAL SOCIETY OF CHEMISTRY

rsc.li/materials-c

View Article Online
DOI: 10.1039/D5TC02429C

ARTICLE

Ag_2S-Engineered Heterojunction Enhances Overall Water Splitting Efficiency of NiS_x Catalysts

Received 00th January 20xx,
Accepted 00th January 20xx

DOI: 10.1039/x0xx00000x

Siqing Li,[‡a] Li Zhou,[‡a] Xinyao Shen, [a] Ying Gu, [a] Yanfeg Tang[*ab] and Minmin Wang[*a]

Ag_2S/NiS_x heterostructures are designed as efficient electrocatalysts for overall water splitting. Ag_2S modifies the electronic structure and induces a large number of active sites. Strong interactions between the interfaces of the heterostructure lead to lower charge transfer resistance and enhance the intrinsic activity of active sites. As expected, Ag_2S/NiS_x demonstrated excellent OER catalytic performance in alkaline environments, with an OER current density of 10, 50, 100 mA cm^{-2} obtained at 1 M KOH at an overpotential of only 42, 137, 180 mV. When used in a two-electrode electrolyzer, Ag_2S/NiS_x can achieve 100 mA cm^{-2} at a low voltage of 1.81 V. This work provides an efficient way to enhance the overall catalytic performance of non-precious metal electrocatalysts.

Introduction

Hydrogen energy is considered to be an ideal energy source due to its sustainability and efficiency[1, 2]. As a pivotal half-reaction in sustainable energy conversion systems, electrocatalytic oxygen evolution reaction (OER) has emerged as a critical frontier in addressing global energy challenges[3-5]. However, the practical implementation of OER faces significant thermodynamic barriers, particularly the high overpotential required to overcome reaction kinetic limitations, which has hindered its commercial viability[6-8]. Recent research has focused on optimizing OER process through designing highly active catalysts[9, 10]. Among various candidate materials, nickel sulfide-based compounds (such as NiS and Ni_3S_2) have garnered particular attention due to their tunable electronic structures, abundant natural reserves, and cost-effectiveness[11, 12].

However, the electrocatalytic activity of nickel sulfide catalysts remains constrained by two critical factors: (1) particle size dependence and structural anisotropy affecting surface-active site exposure, and (2) intrinsic limitations in electronic conductivity that hinder efficient charge transfer during oxygen evolution reactions (OER)[13, 14]. Recent advances suggest that constructing hierarchical heterostructures through strategic material hybridization offers a promising solution pathway[15-17]. The interfacial charge redistribution at phase boundaries can effectively modify local electronic environments through built-in electric fields[18-20]. This synergistic effect not only reduces energy barriers in potential-determining steps but also enhances overall conductivity by creating interconnected electron transport pathways[21, 22].

In this study, a heterojunction catalyst comprising superionic Ag_2S and nickel sulfide (NiS_x) phases ($Ag_2S/NiS/Ni_3S_2$) was synthesized via electrodeposition followed by low-temperature vulcanization. Further characterization revealed that the heterojunction formation induced optimized electronic configurations at the interface, facilitating efficient charge carrier migration between the Ag_2S and NiS_x phases. This structural configuration demonstrated remarkable electrocatalytic efficiency, achieving a low overpotential of 180 mV @100 mA cm^{-2} in OER. Particularly noteworthy was the significantly low battery voltages of 1.81 V to facilitate full water splitting at 100 mA cm^{-2}. Systematic XPS analysis verified electron redistribution patterns (Ag $3d_{5/2}$ binding energy downshifted 0.4 eV, Ni $2p_{3/2}$ upshifted 0.2 eV), confirming strong interfacial electronic coupling. Furthermore, the material exhibited negligible performance degradation during a 100-hour stability test, thereby presenting a novel approach for the commercial deployment of non-precious metal electrocatalysts.

Results and discussion

The Ag_2S/NiS_x was developed by bottom-up strategy. As detailed in Supplementary Material Scheme. S1, the silver nanosheets grown on nickel foam (Ag/NF) and then nickel hydroxide specie modified on the Ag/NF by electrodeposited. Finally, the Ag_2S/NiS_x heterojunction was obtained by low temperature vulcanization[23, 24]. The detailed synthetic procedures were shown in experimental section. The phase purity was determined by XRD, as shown in Fig. 1a. The characteristic peaks at 36.9°, 45.7° and 53.3° correspond to (2 0 0), (2 1 1) and (2 2 0) planes of Ag_2S (JCPDS No. 71-0995), while the peaks at 32.7°, 40.9° and 48.9° match NiS (JCPDS No. 86-2280). Additionally, the peaks at 30.5°, 34.9°,53.8° and 73.1° are

[a] School of Chemistry and Chemical Engineering, Nantong University, 9 Seyuan Road, Nantong, 226019, Jiangsu, P. R. China.
[b] School of Chemical Engineering and Materials Science, Taizhou university, Taizhou, 225300, China.
* Corresponding email: mmwang0528@ntu.edu.cn; 2005110005@tzu.edu.cn.
‡ These authors contributed equally to this work.
Supplementary Information available: [details of any supplementary information available should be included here]. See DOI: 10.1039/x0xx00000x

View Article Online
DOI: 10.1039/D5TC02429C

ARTICLE

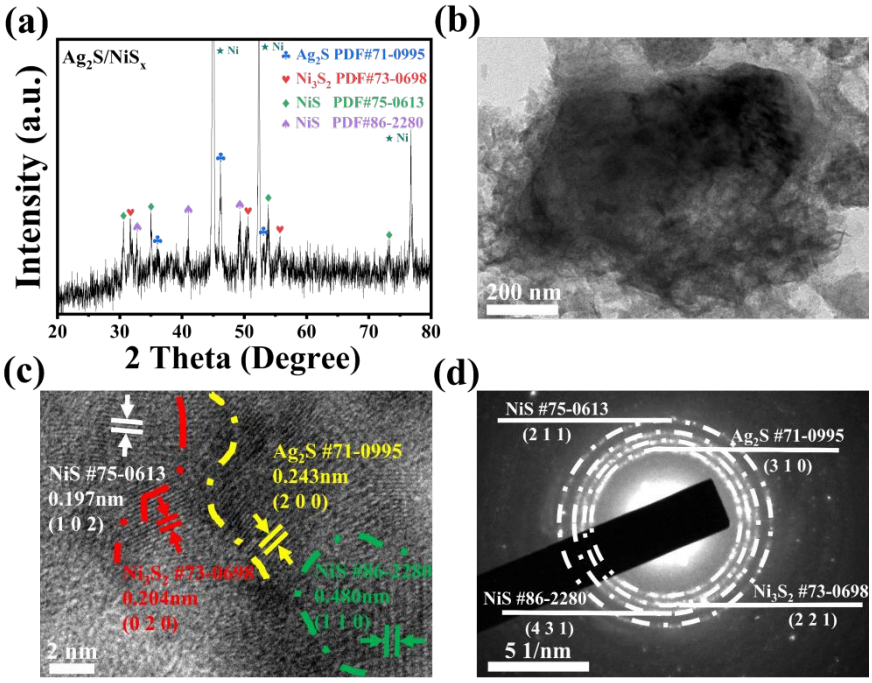

Fig. 1. (a) PXRD pattern of developed Ag_2S/NiS_x. (b) TEM and (c) HRTEM images of Ag_2S/NiS_x nanoheterojunction. (d) The corresponding SAED pattern of Ag_2S/NiS_x nanoheterojunction.

attributed to NiS (JCPDS No. 75-0613) and the peaks at 31.6°, 50.2° and 55.5° correspond to Ni_3S_2 (JCPDS No. 73-0698). Notably, the absence of metallic Ag (38.2°) peak confirms complete vulcanization (Fig. S1a). In Fig. S1b, the morphologies of the precursor silver nanosheets were characterized by SEM. The detailed morphology of Ag_2S/NiS_x heterojunction was analysed by TEM and HRTEM. As depicted in Fig. 1b, the Ag_2S/NiS_x exhibits ultra-thin nanosheets morphology and the heterojunction interface was determined by HRTEM image. As shown in Fig. 1c, the lattice spacing of 0.243 nm corresponds to the (2 0 0) interface of Ag_2S, while the adjacent 0.197 nm and 0.480 nm spacing matches well with the (1 0 2) plane of NiS (PDF#75-0613) and (1 1 0) of NiS (PDF#86-2280), and the lattice spacing of 0.204 nm corresponds to the (0 2 0) interface of Ni_3S_2 (PDF#73-0698), confirming the successful construction of phase boundaries. Notably, the intimate interfacial contact between these two sulfides is evidenced by the continuous lattice fringes observed at the junction area. High-angle annular dark-field scanning TEM (HAADF-STEM) and corresponding element mapping measurement was used to determine the elemental composition information of Ag_2S/NiS_x material, which proved that Ag, Ni, and S elements all existed in the material (Fig. S2). Further analysis using selected area electron diffraction (SAED) pattern revealed distinct concentric polycrystalline diffraction rings (Fig. 1d), which could be indexed to the overlapping crystallographic planes of Ag_2S, NiS, and Ni_3S_2. The co-existence of multiple diffraction patterns corroborates the formation of well-defined heterointerfaces between different sulfide phases which match well with the XRD characterizing.

The chemical composition and electronic structure of Ag_2S/NiS_x heterojunction were systematically characterized by high resolution X-ray photoelectron spectroscopy (XPS). The full spectrum scanning in Fig. S3 verifies the simultaneous existence of Ag, Ni and S. The high- resolution photoelectron spectra of Ag 3d exhibit peaks at 374.2 eV and368.2 eV, corresponding to Ag $3d_{3/2}$ and Ag $3d_{5/2}$, respectively. The Ag 3d bimodal shifts 0.4 eV to the direction of low binding energy, indicating the electron transfer from NiS_x matrix Ag_2S (Fig. 2a). This charge redistribution is further corroborated by ultraviolet photoelectron spectroscopy (UPS) measurements (Figure S4). The UPS spectra conclusively demonstrate the successful construction of the Ag_2S/NiS_x heterojunction via controlled sulfur diffusion, revealing that electron transfer from NiS_x to Ag_2S. The detailed analysis of the bonding characteristics (Fig. 2b) shows that the double peaks in the Ni 2p orbital binding energy at 855.7 eV and 873.4 eV are assigned to $2p_{3/2}$ and $2p_{1/2}$, while the double peaks at 873.4 eV and 879.8 eV confirm the coordination bonds between nickel-sulfur species[25]. We also provide a high-resolution spectrum of S 2p, and the S-O component also indicates the presence of NiS_x[26]. In the S 2p

View Article Online
DOI: 10.1039/D5TC02429C

ARTICLE

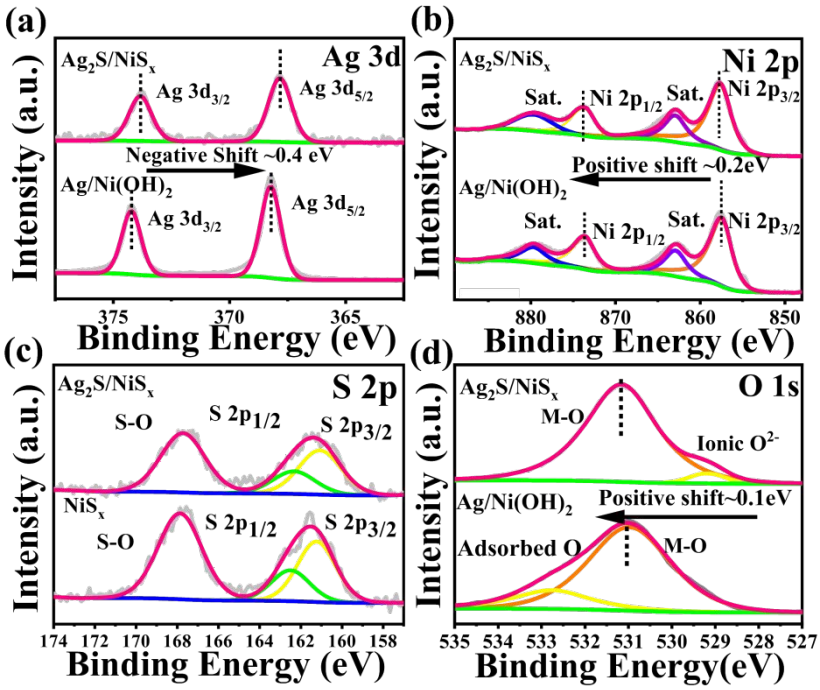

Fig. 2. High-resolution XPS spectra of Ag_2S/NiS_x, $Ag/Ni(OH)_2$, NiS_x: (a) Ag 3d, (b) Ni 2p, (c) S 2p and (d) O 1s.

spectrum, the characteristic peak of $2p_{3/2}$ at 161.26 eV is attributed to the S-M bonding, while the $2p_{1/2}$ peak at 162.56 eV is assigned to unsaturated S atoms in the Ag_2S/NiS_x system, confirming the formation of sulfur vacancies (Fig. 2c)[27]. The high-resolution energy spectrum of O 1s exhibited a prominent peak centred at 531.2 eV, which unequivocally verifies the existence of -OH functional groups. Conversely, the peak observed at 528.4 eV is attributed to defective oxygen atoms within the nickel sulfide (Fig. 2d)[28].

The OER performance of the Ag_2S/NiS_x nanoheterojunction electrode was evaluated in 1 M KOH solution utilizing a standard three-electrode configuration. As depicted in Fig. 3a, the polarization curve was acquired at a scanning rate of 5 mV s^{-1}, and the corresponding current densities have been normalized to the geometric surface area (1 cm^2) for accurate comparison and analysis. The fabricated Ag_2S/NiS_x heterojunction electrode necessitates ultralow overpotential of 180 mV to drive oxygen evolution at 100 mA cm^{-2}, significantly surpassing $Ag/Ni(OH)_2$ (398 mV) and NiS_x (212 mV), respectively. The onset potential of oxidation peaks for both Ag_2S/NiS_x and its precursor is identified at 1.34 V vs. RHE, corresponding to the characteristic Ni^{2+}/Ni^{3+} redox transition. Notably, as depicted in Fig. 3b, we have conducted a comparative analysis of the overpotential exhibited by the synthesized catalysts at various current densities, including 10, 50, and 100 mA cm^{-2}. The Ag_2S/NiS_x electrode demonstrated significantly lower overpotentials of 42, 137, and 180 mV, respectively, which are representing 82.1%, 52.4%, and 41.9% reductions compared to RuO_2 electrode (corresponding values of 234, 288, and 310 mV)[29]. This voltage-dependent behavior suggests that the surface-anchored NiS_x domains facilitate the formation of higher-valent Ni species (Ni^{3+}/Ni^{4+}), which are widely recognized as the active centers for oxygen evolution reaction[30-32]. Furthermore, as depicted in Fig. 3c, the fabricated Ag_2S/NiS_x electrode exhibits a minimal Tafel slope of 64.38 mV dec^{-1}, signifying the superior oxygen evolution kinetics possessed by the Ag_2S/NiS_x material.

To further understand the mechanism of enhanced OER performance of the prepared electrode, the electrochemically active area (ECSA) was assessed by cyclic voltammetry. In Fig. 3d and Fig. S5a-c, the Ag_2S/NiS_x electrode presents the high ECSA of 2182.75 cm^2 with C_{dl} value of 87.31 mF cm^{-2}, which is higher than $Ag/Ni(OH)_2$ (1808.25 cm^2, 72.33 mF cm^{-2}) and NiS_x (910.5 cm^2, 36.42 mF cm^{-2}) electrodes. According to the characterization results of electrochemical impedance spectroscopy the Nyquist curve in Fig. 3e clearly shows the synthesized Ag_2S/NiS_x heterojunction electrode has significant optimization of charge transfer characteristics. The charge transfer resistance (R_{ct}) of the composite is reduced to 3.9 Ω, which is significantly lower than that of its precursor $Ag/Ni(OH)_2$ (14.2 Ω) and 6.4 Ω of NiS_x. Compared to $Ag/Ni(OH)_2$, the Rct value of the composite decreased by 72%, while it showed a reduction of over 39% compared to pure NiS_x. This

View Article Online
DOI: 10.1039/D5TC02429C

ARTICLE

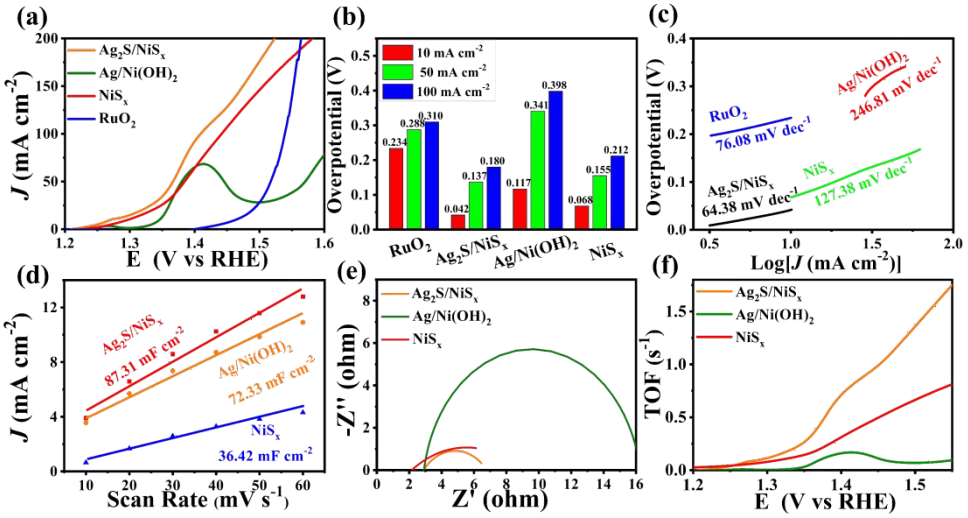

Fig. 3. (a) Polarization curves of Ag_2S/NiS_x, $Ag/Ni(OH)_2$, NiS_x and RuO_2. (b) Overpotentials Bar Graph. (c) Tafel plots and (d) The value of the double layer capacitances. (e) Nyquist plots of Ag_2S/NiS_x, $Ag/Ni(OH)_2$, NiS_x at an overpotential of 280 mV. (f) The calculated turnover frequency of as-prepared electrodes in OER.

breakthrough improvement of interface charge transfer characteristics may be due to the synergistic effect of the formation of Ag_2S and NiS_x heterojunction interface. The intrinsic catalytic activity was further evaluated by determining the turnover frequency (TOF) through chronoamperometric measurements. As shown in Fig. 3f, when operated at an overpotential of 200 mV, the Ag_2S/NiS_x hybrid catalyst demonstrates a TOF value of 0.88 s^{-1}, which shows a remarkable 1.1-fold enhancement compared to pure NiS_x (0.42 s^{-1}). This exceptional activity of the Ag_2S/NiS_x hybrid can be attributed to its unique heterostructure configuration.

After subjecting the Ag_2S/NiS_x electrode to extensive cyclic voltammetry testing over 1000 cycles, analysis of the polarization curves reveals exceptional structural persistence (Fig. S6a). Furthermore, we conducted a rigorous investigation into the long-term stability of two-dimensional Ag_2S/NiS_x nanocomposites, employing a potentiostatic testing approach under a constant overpotential. As shown in Fig. S7a, under a constant overpotential of 1.43 V (vs. RHE), the electrode maintained 96.39 % of its initial current density over a 100-hour continuous operation period. Meanwhile, post-test characterization revealed preserved structural integrity with no detectable phase separation or agglomeration (Fig. S8). This exceptional stability can be attributed to the synergistic effects derived from the unique 2D heterostructure, where the interfacial electron coupling between Ag_2S and NiS_x effectively inhibited metal dissolution and surface oxidation. This stability enhancement was systematically verified through post-test characterization. Following extended OER stability testing, phase analysis revealed the exclusive persistence of Ni_3S_2, underscoring its critical function in maintaining the material's structural integrity under prolonged electrochemical operation (Fig. S9a). XPS analysis revealed significant changes in oxygen species, particularly the emergence of a distinct -OH peak at 533.13 eV. This observation aligns with our hypothesis that prolonged operation under alkaline conditions facilitates progressive hydroxide accumulation on the catalyst surface. Such surface modification explains the diminished sulfur signal intensity in corresponding XPS spectra, while the electronic structure evolution of Ag, Ni, and S elements synergistically optimizes the catalytic active sites (Fig. S9b-f). Finally, comparative studies with monometallic sulfides demonstrated at least 1.2-fold improvement in activity and durability, highlighting the advantage of our design strategy. Additionally, the Ag_2S/NiS_x electrode demonstrates superior catalytic performance compared to most recently reported OER electrocatalysts, as evidenced in Table S1.

We also investigated the HER performance of Ag_2S/NiS_x nanoheterojunction electrode in alkaline condition. As shown in Fig. 4a, when the geometric area of the working electrode is normalized to 1 cm^2, the overpotential of the Ag_2S/NiS_x heterojunction at 100 mA cm^{-2} is only 268 mV, which is lower than that of its precursor $Ag/Ni(OH)_2$ (353 mV) and NiS_x (316 mV) decreased by 24.1% and 15.2%, respectively. This significant performance improvement is universal under different current densities (Fig. 4b), showing the lowest over potential value in the range of 10-100 mA cm^{-2}. The intrinsic catalytic activity of the materials was verified by multi-level characterization. Tafel slope analysis shows that Ag_2S/NiS_x electrode has excellent kinetic characteristics of 103.37 mV dec^{-1} (Fig. 4c), implying that

View Article Online
DOI: 10.1039/D5TC02429C

ARTICLE

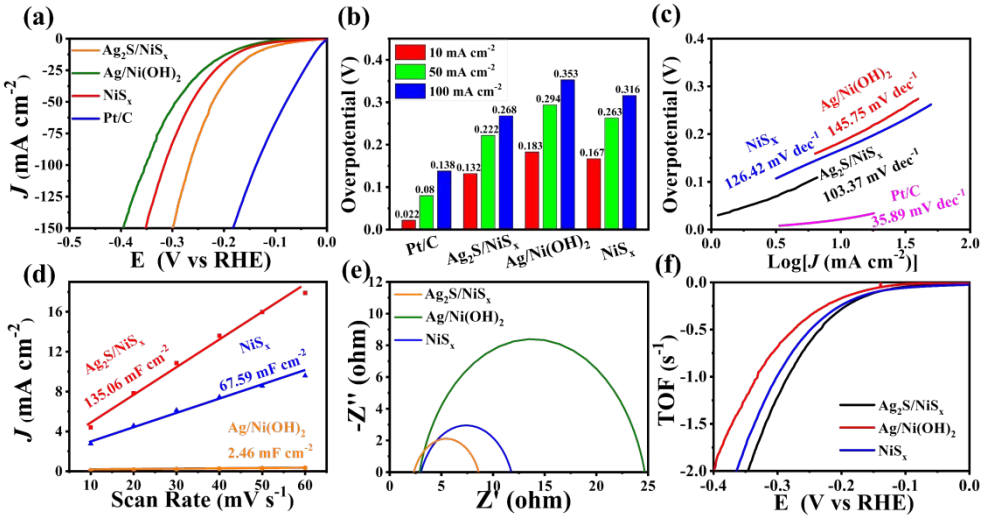

Fig. 4. (a) Polarization curves of Ag_2S/NiS_x, $Ag/Ni(OH)_2$, NiS_x and Pt/C. (b) Overpotentials Bar Graph. and (c) Tafel plots. (d) The value of the double layer capacitances. (e) Nyquist plots of various catalysts at an overpotential of 150 mV. (f) The calculated turnover frequency of as-prepared electrodes in HER.

it follows the Volmer Heyrovsky reaction mechanism[33]. The electrochemical active area test and Nyquist spectrum (Fig. 4d-e and Fig. S5d-f) jointly confirmed that the heterojunction had higher active site density and lower charge transfer impedance, which provided a structural basis for improving HER performance. It is worth noting that although the TOF test (Fig.4f) shows that the intrinsic catalytic ability of Ag_2S/NiS_x is similar to that of NiS_x, but constructing a hierarchical nanostructure by incorporating silver nanosheets to increase the specific surface area enhanced the reaction activity (about

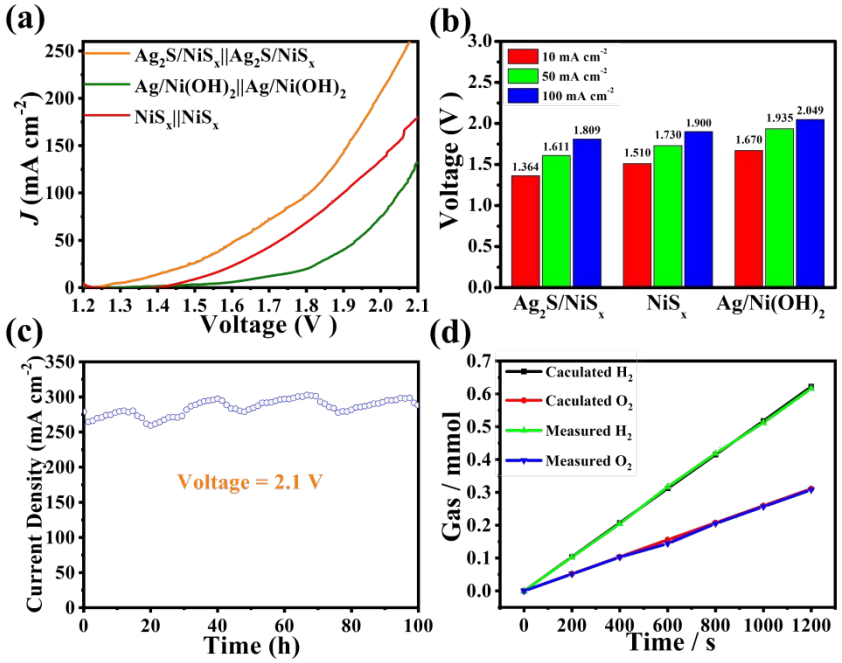

Fig. 5. (a) LSV curves of obtained samples in 1 M KOH. (b) Corresponding cell voltages at 10, 50 and 100 mA cm^{-2}. (c) Long-term Stability testing of Ag_2S/NiS_x at the voltage of 2.1 V. (d) The measured and calculated amounts of H_2 and O_2 gases versus time measured at a constant current density of 100 mA cm^{-2}.

View Article Online
DOI: 10.1039/D5TC02429C

ARTICLE

1.2 times higher), achieving a significant breakthrough in apparent activity levels. In terms of stability assessment (Fig. S6b and Fig. S7b), the Ag_2S/NiS_x heterojunction electrode remains 98.54% after 100 hours of continuous testing.

According to the excellent performance of Ag_2S/NiS_x electrode in the OER and HER reactions, total water decomposition system of electrode was constructed in 1 M KOH electrolyte. The cell voltage required for the system to achieve 10, 50 and 100 mA cm^{-2} current density is 1.36, 1.61 and 1.81 V respectively (Fig. 5a-b), which is significantly superior to most transition metal sulfide-based catalysts reported in the literature (Table. S2). It is noteworthy that the two-electrode system still maintains an initial efficiency of ~100% after 100 hours of continuous operation at a high current density of 250 mA cm^{-2} (Fig.5c). This excellent stability is due to the strong interaction between Ag_2S and NiS_x, which effectively avoids the structural collapse of the catalyst during long-term operation. Through Faraday efficiency test, it is found that under the condition of 100 mA cm^{-2} constant current, the H_2/O_2 molar ratio is stable and close to 2:1 (Fig. 5d), and the average Faraday efficiency is 98.7 $\pm$ 0.5%, which further confirms the high efficiency of charge transfer in the electrolysis process.

Conclusions

In summary, a composite structure of Ag_2S/NiS_x nanoheterojunction was developed. The hierarchical architecture creates abundant active interfaces between Ag_2S and NiS_x phases, promoting synergistic charge transfer at the nanoscale heterojunctions. In the OER test of the Ag_2S/NiS_x catalyst prepared by us, the current density of 10 mA cm^{-2}, 50 mA cm^{-2} and 100 mA cm^{-2} can be obtained by overpotentials of 42 mV, 137 mV and 180 mV to drive oxygen evolution reactions. As a dual-function catalyst, Ag_2S/NiS_x exhibits outstanding performance in the overall electrolytic water process. The current density of 10 mA cm^{-2}, 50 mA cm^{-2}, and 100 mA cm^{-2} can be driven by the battery voltage of 1.36 V, 1.61 V and 1.81 V. During the extensive long-term stability assessment, the fabricated Ag_2S/NiS_x electrode demonstrated remarkable endurance and stability over an extended period. The discoveries and insights gathered from this study have the potential to pave novel pathways for the development and investigation of collaborative bifunctional electrocatalysts targeted for extensive industrial hydrogen generation.

Conflicts of interest

There are no conflicts to declare.

Data availability

The authors declare that all the data generated during this study are available within the paper and its ESI.

Acknowledgements

This work is supported by National Natural Science Foundation of China (No. 22075152) and Postgraduate Research & Practice Innovation Program of Jiangsu Province (134424608108).

Notes and references

1. P. M. Bodhankar, P. B. Sarawade, P. Kumar, A. Vinu, A. P. Kulkarni, C. D. Lokhande and D. S. Dhawale, *Small*, 2022, **18**, 2107572.
2. Y. Du, H. Chen, Z. Huang, X. He, W. Fang, W. Li and L. Zhao, *ACS Applied Energy Materials*, 2020, **3**, 687-694.
3. Y. Zhang, Z. Zhang, X. Zhang, J. Li and R. Guo, *International Journal of Hydrogen Energy*, 2025, **102**, 304-320.
4. M. Rong, Y. Mo, Z. Cao, X. Ma, S. Wang and H. Zhong, *International Journal of Hydrogen Energy*, 2022, **47**, 18688-18699.
5. Y. Guo, Z. Yu, B. He and P. Chen, *Chinese Chemical Letters*, 2025, **36**, 111010.
6. M. Guo, R. Deng, C. Wang and Q. Zhang, *Journal of Energy Chemistry*, 2023, **78**, 537-553.
7. X. M. C. Ta, T. Tràn-Phú, T. K. A. Nguyen, M. Chatti and R. Daiyan, *Appl Phys Rev*, 2024, **11**, 021321.
8. Y. Li, Q. Li and S. Peng, *Journal of Colloid and Interface Science*, 2025, **689**, 137209.
9. P.-F. Guo, Y. Yang, B. Zhu, Q.-N. Yang, Y. Jia, W.-T. Wang, Z.-T. Liu, S.-Q. Zhao and X. Cui, *Carbon Energy*, 2024, **6**, e532.
10. X. Ren, C. Wei, Y. Sun, X. Liu, F. Meng, X. Meng, S. Sun, S. Xi, Y. Du, Z. Bi, G. Shang, A. C. Fisher, L. Gu and Z. J. Xu, *Advanced Materials*, 2020, **32**, 2001292.
11. Z. Li, M. Hu, P. Wang, J. Liu, J. Yao and C. Li, *Coordination Chemistry Reviews*, 2021, **439**, 213953.
12. J. Chen, X. Xu, R. Mao, C. Wang, H.-Y. Hsu, Z. Yin, M. A. Buntine, A. Suvorova, M. Saunders, Z. Shao and G. Jia, *Journal of Materials Chemistry A*, 2024, **12**, 27364-27372.
13. Y. Chen, Y. Fan, Z. Cui, H. Huang, D. Cai, J. Zhang, Y. Zhou, M. Xu and R. Tong, *International Journal of Hydrogen Energy*, 2023, **48**, 27992-28017.
14. Y. Bai, P. Fu, Y. Gan, Q. Cheng, J. Wang, X. Guo, W. Xiong, X. Cheng, F. Zheng and J. Zhang, *Journal of Colloid and Interface Science*, 2024, **670**, 364-372.
15. C. Lin, H. Lu, X. Ren, B. He, X. Peng and P. Chen, *Chemical Engineering Journal*, 2025, **509**, 161475.
16. G. Zhou, N. Zhang, Z. Huang, J. He, J. Zhu, X. Ren, Y. Tong, H. Wang and P. Chen, *Chemical Engineering Journal*, 2025, **503**, 158619.

View Article Online
DOI: 10.1039/D5TC02429C

17. Y. Wu, Z. Yu, Y. Tong, C. Lin, N. Zhang and P. Chen, *Advanced Functional Materials*, 2025, 2502104.
18. Y. Sun, S. Zhou, N. Yang, H. Shen, X. Yang, L. Zhang, X. Xiao, B. Jiang and L. Zhang, *Journal of Colloid and Interface Science*, 2025, **688**, 1-10.
19. M. Cao, B. Li, Y. Cao, Y. Li, R. Tian, Q. Shen, W. Xie and W. Gu, *ACS Applied Materials & Interfaces*, 2025, **17**, 15259-15273.
20. S. Adhikari, S. N. Steinmann, M. Arunachalam, S. H. Kang and D.-H. Kim, *Small*, 2024, **20**, 2311548.
21. X. Zeng, X. Bu, H. Chen, Z. Huang, W. Fang, D. Wang, X. He, X. Du, W. Li, H. Zhang and L. Zhao, *Composites Part B: Engineering*, 2024, **287**, 111838.
22. G. Jin, X. Ren, C. Lin, B. He and P. Chen, *Journal of Colloid and Interface Science*, 2025, **687**, 432-438.
23. Y. Dong, Y. Su, Y. Hu, H. Li and W. Xie, *Small*, 2020, **16**, 2001529.
24. P. Yi, Y. Song, Z. Liu, P. Xie, G. Liang, R. Liu, L. Chen and J. Sun, *Advanced Composites and Hybrid Materials*, 2023, **6**, 228.
25. G. Zhao, Y. Xing, Y. Liu, X. Wang, B. Zhang, L. Mu, W. Liao and X. Xu, *Materials Today Chemistry*, 2023, **34**, 101758.
26. Y. Zhou, X. Yang, S. Xi, B. He and Y. Song, *International Journal of Hydrogen Energy*, 2020, **45**, 11138-11147.
27. M. Chen, Q. Su, N. Kitiphatpiboon, J. Zhang, C. Feng, S. Li, Q. Zhao, A. Abudula, Y. Ma and G. Guan, *Fuel*, 2023, **331**, 125794.
28. X. Zhao, J. Wang, L. Lian, G. Zhang, P. An, K. Zeng, H. He, T. Yuan, J. Huang, L. Wang and Y.-N. Liu, *ACS Catalysis*, 2023, **13**, 2326-2334.
29. H. Wang, H.-W. Lee, Y. Deng, Z. Lu, P.-C. Hsu, Y. Liu, D. Lin and Y. Cui, *Nature Communications*, 2015, **6**, 7261.
30. L. Dai, Z.-N. Chen, L. Li, P. Yin, Z. Liu and H. Zhang, *Advanced Materials*, 2020, **32**, 1906915.
31. Y. Wang, J. Liu, Y. Liao, C. Wu and Y. Chen, *Journal of Alloys and Compounds*, 2021, **856**, 158219.
32. J. Yu, Q. Li, N. Chen, C.-Y. Xu, L. Zhen, J. Wu and V. P. Dravid, *ACS Applied Materials & Interfaces*, 2016, **8**, 27850-27858.
33. B. Tian, L. Sun, Z. Zeng and D. Ho, *Journal of Materials Chemistry A*, 2024, **12**, 22082-22091.

The authors confirm that the data supporting the findings of this study are available within the article and its supplementary materials.